ISSN 1063-7745, Crystallography Reports, 2025, Vol. 70, No. 6, pp. 878–882. © Pleiades Publishing, Inc., 2025.

DIFFRACTION AND SCATTERING OF IONIZING RADIATIONS

Problems with Synchrotron Radiation Phase-Contrast Imaging of Micro-objects in Crystals

T. S. Argunova[a,*], V. G. Kohn[b], and J.-H. Lim[c]

[a] *Ioffe Institute, Russian Academy of Sciences, St. Petersburg, 194021 Russia*

[b] *National Research Centre "Kurchatov Institute," Moscow, 123182 Russia*

[c] *Pohang Light Source, Pohang, 37673 South Korea*

**e-mail: argunovat@mail.ioffe.ru*

Received July 18, 2025; revised August 11, 2025; accepted August 11, 2025

Abstract—Problems in experimental study of real crystal structures using phase-contrast imaging with synchrotron radiation (SR) are discussed, and methods for their solution are proposed. The experiment was performed at the Pohang Light Source in Pohang City, Republic of Korea. Diamond crystals were examined. The capabilities of the method in studying weak changes in the crystal density under conditions of spatially inhomogeneous beam intensity, beam statistical noise, and detector imperfections were analyzed. Images of various shapes and sizes were obtained, which indicated the presence of defects. However, a more detailed analysis is required to identify these defects.

DOI: 10.1134/S1063774525601261

INTRODUCTION

X rays have been widely applied after their discovery in 1895, in two fields at once: diffraction from the crystal lattice and imaging of the internal structure of materials by the nonuniform absorption method. The research methods in these fields are still being developed and improved. The spatial period of electromagnetic field oscillations in hard synchrotron radiation (SR) with a photon energy of 10–20 keV is comparable with the lattice period (specifically, not much smaller than this parameter). Therefore, the diffraction angles are relatively large, which is convenient for experiments. At the same time, the refraction of X-rays at the interface between two media is fairly weak, and rays pass through an object barely changing their trajectory. Images of noncrystalline objects with sizes differing not much from the human body sizes, as well as weakly absorbing crystals beyond the Bragg conditions, are obtained without distortions and are determined by only absorption. In other words, optically dense regions in an object can clearly be seen.

However, with a decrease in the sizes of inhomogeneities in the illuminated object, the absorption contrast becomes weak. In this case, a clearer image can be obtained in coherent radiation by changing the phase of the SR wave function. At a small distance from the object, the detector does not record the phase, but, with increasing distance, a change in phase is transformed into an intensity change, and one can obtain a phase-contrast image [1, 2]. In this way, researchers analyze both small objects in air [3–7] and various small changes in electron density in crystals [8–14]. Sharp changes in density arise in pores, for example, in dislocation micropipes [10–12] in silicon carbide crystals, as well as in the spherical pores accumulating vacancies in such crystals as sapphire, silicon carbide, etc. [13]. Pores with relatively large sizes may have most diverse shapes, not only spherical [15, 16].

The study of such objects is partially simplified by the fact that their shape is approximately known, and one has only to determine their size. Also, using numerical simulation, one can easily gain a complete understanding of how these images are formed [13, 14]. Recently, we could identify growth steps on the surface of sapphire crystals and determine their height: ~1 μm [17–20]. However, in other crystals, for example, in diamond, such defects are absent, but there may be other defects [21], which have not yet been studied by the phase-contrast method. The results of such study are presented for the first time in this paper. The corresponding problems are discussed as well.

Two-dimensional coordinate detectors are used in beamlines at modern SR sources to record images; these detectors may have bad pixels. The SR beam itself may have finite sizes and relatively high inhomogeneity, as well as statistical noise. All these factors deteriorate the quality of experimental results and call for their careful analysis by mathematical methods of image processing.

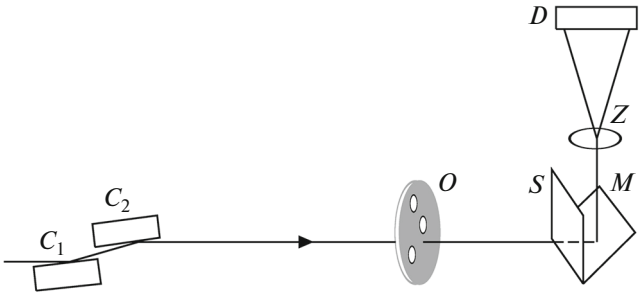

Fig. 1. Schematic of the experiment: (C_1, C_2) 111 Si monochromator crystals, (O) object of study, (S) scintillator, (M) mirror made of Si crystal, (Z) optical objective, and (D) detector.

SCHEME OF THE EXPERIMENT AND METHOD OF STUDY

The scheme of the experiment to visualize small inhomogeneities in crystals barely differs from the scheme of imaging of small objects in air. It contains a radiation source, a monochromator, a crystal, and a detector (Fig. 1). Diamond crystals were studied on the 6C (Biology and Medical Imaging) beamline of the Pohang Light Source in the Pohang City, Republic of Korea. The radiation of a wiggler with photon energy of 25 keV, which is in the beginning of the range of available energies (23–50 keV) at this beamline, was used. The beamline is equipped with an Orca-Fusion detector (Hamamatsu Photonics, Japan), which allows one to perform measurements at any illuminance level, but especially under conditions of low illuminance. The low level of detector readout noise indicates that even small numbers of photons from the illuminated object are not lost in spurious noise but detected quantitatively. The detector wrote data into tiff files as integers 2 bytes (16 bits) long and formed a square image with 2304 pixels per side. The effective linear pixel size was 0.325 μm. This value is obtained by recalculating the real pixel size (6.5 μm) after dividing by 20. Specifically this magnification was obtained by transforming SR into optical light in the crystalline scintillator, after which the image was magnified by a factor of 20 using an optical objective.

As a result, the linear size of the image that could be fixed by the detector without scanning was 750 μm. This size was comparable to the effective size of the SR beam formed by a system of slits at a specified objective magnification. The radiation incident on the detector gave an inhomogeneous image even in the absence of a sample. Under these conditions, measurements must be performed in three stages. Primarily, we recorded the dark detector image (the incident SR beam was blocked by a shutter). Even in this case the detector yields an image containing statistical inhomogeneities, as well as bad pixels. It is necessary to make sure that the interference intensity is low and that broken pixels cannot affect significantly the result.

The image of an empty SR beam was recorded in the second stage. Such images must be recorded several times, because the beam contains shot noise, which must be estimated. This issue will be considered in more detail below. The image of a crystal in the SR beam is recorded in the third stage. In all cases the detector records the radiation intensity. Obviously, the crystal image is obtained jointly with the empty beam image, which contains also the image of the dark detector (including the scintillator). To exclude spurious images from crystal images, one must extract number matrices from the files and divide the crystal matrix by the empty beam matrix.

This procedure is equivalent to the subtraction of the empty beam contrast from the contrast of crystal in this beam, if both contrasts are small. As a result, there remains a crystal image in an arbitrarily flat beam, which is necessary for processing the phase-contrast image and solving the inverse problem in order to obtain quantitative information about structural defects. If the crystal under study does not yield an image, there must be a homogeneous background. In fact, the background is irregular because of the beam statistical noise. This noise can be characterized by a contrast (visibility), which will defined as follows: $V = (F_{ma} - F_{mi})/(F_{ma} + F_{mi})$, where F_{ma} and F_{mi} are the maximum and minimum values in the matrix image. In other words, the crystal image contrast should exceed this noise; otherwise, the information will be incorrect. The noise level can be analyzed by dividing the matrices of the empty SR beam, obtained in measurements at different instants.

It is of interest that noise can be sharply reduced in amplitude by averaging the experimental matrix using the method for calculating convolution with localized function of different types. The most convenient candidates are the Gaussian function and a function that is nonzero in a square of specified size. The calculation results showed that this procedure makes it possible to reduce sharply the amplitude of the background noise, but the noise cannot be removed completely. The point is that, along with the short-period noise, the beam contains a long-period noise, which is not completely suppressed in this way, although its amplitude becomes much smaller. This noise image may distort the image of objects in crystal because it is spurious. Correspondingly, one should pay attention to only the contrast exceeding the noise contrast of the SR beam.

MEASUREMENT RESULTS AND THEIR PROCESSING

The measurement results were saved by the detector in the form of 16-bit tiff images. The tiff format makes it possible to save e-books of any degree of

complexity, but it has also a simpler version, which records a matrix of integers in range from 0 to 65535, each number two bytes long, without compression. Specifically this version is used to save detector readings. In the first stage, it is necessary to analyze the detector readings with a blocked beam, i.e., the dark detector readings, and make sure that the detector is correctly tuned and the experimental conditions are satisfactory.

The dark detector reading themselves are used nowhere, but they affect other readings. Therefore, it is necessary to make sure that this influence is not critical. All results were processed using our own programs, written in the VKACL language [22]. The interpreter for this language, all programs written in it, and the corresponding documentation are available at the aforementioned website. A special program extracts a number matrix from a tiff file and performs its preliminary analysis. In particular, one can easily obtain minimum, mean, and maximum values, as well as the coordinates of the first largest values.

The dark detector should yield zeros, but this does not occur. The matrix has nonzero values. Moreover, if the mean may be fairly small (it was equal to 100 in our case), the maximum value may be fairly large. In the performed study it was equal to 3605, and the values following it were 2461, 2436, and 2212. It is known that any coordinate detector has bad pixels. The number of these pixels is not very large, but they are always present. Their readings should be disregarded. They generally show values in no way matched with neighbors; clusters of bad pixels also occur, but more rarely.

In a scientific paper, it is fairly difficult to show the entire square matrix 2304 px in size without any specific image. Therefore, Fig. 2 presents a square fragment with a linear size of 200 px; the pixel having maximum value is located at the center. Here, it is convenient to present the natural logarithm of values, with indication of the specific coordinates of the area in the large matrix. In this case, one can see more clearly how both large and small values change. The initial matrix was normalized in the range from 0 to 1, and the logarithms of the minimum and maximum values are shown in the caption. Since the bad pixels have small values, no special measures were taken to take into account the dark detector readings.

In the next stage, 10 images of SR beam without a crystal were measured. The beam turned out to be inhomogeneous in a square with a linear size of 750 μm. Its image resembles approximately the middle part of the Gaussian function image but has some artifacts. To form a homogeneous background, it is necessary to divide the matrix of detector readings with a sample by the matrix of empty SR beam. However, all crystal images have statistical noise, which should not be confused with the image of the crystal itself. To estimate the noise level, it is reasonable to divide

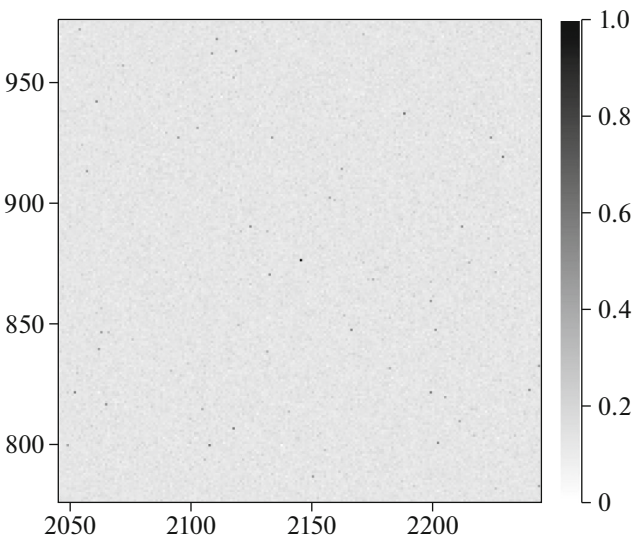

Fig. 2. Fragment of distribution of the natural logarithm of the number of dark detector references with a size of 200 × 200 px and a center corresponding to the coordinates of the largest pixel, specifically, $x = 2145$, $y = 877$. The numbers of pixels in the initial detector matrix 2304 × 2304 in size are plotted along the axes. The color map is shown for the normalized array. The values of the logarithm minimum and maximum in the real array are 4.094 and 8.190, which corresponds to the reference numbers of 60 and 3605.

the empty beam matrices from different measurements. In this case, it is only the noise image that remains. The noise images themselves can be separated into short and long ones. The former change rapidly and have a short period, while the latter change slowly and have a long period.

The short noise can be significantly reduced using the method of averaging the matrix over some size by calculating the matrix convolution with some function, which is nonzero in a limited region. Generally, the Gaussian function is used to this end. However, when averaging noise, the function that is nonzero in a specified square, where it is equal to a constant and has a unit integral, also deserves attention. The convolution with this function is calculated fairly rapidly and provides a clearer contrast. Averaging was performed over a square with a linear size of 9 px, corresponding to the coherence length of 3 μm, which is consistent with the data of many previous experiments [10–14, 17–20].

According to the data of four calculations with different matrices, the mean obtained after the division is unity with a relatively high accuracy, and the mean contrast is 0.095 for the initial matrices and 0.021 for the averaged matrices. Figure 3 presents the averaged matrix for one of the calculations. Note that the specific pattern of matrices has a random character, and all calculated matrices are different. However, their statistical characteristics are relatively close, and the spread of values does not exceed 10%. The specific

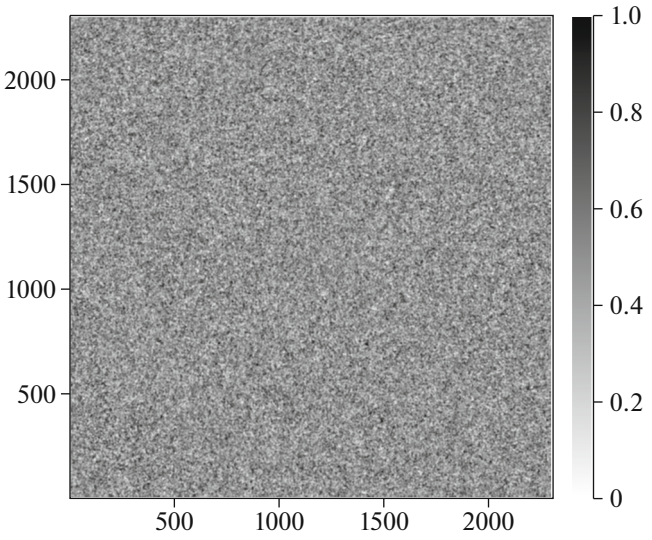

Fig. 3. Ratio of the detector readings on a 2304 × 2304 matrix for two measurements of the SR beam without the crystal studied, after averaging the matrix by calculating the convolution with the matrix whose values differ from zero and equal to each other in a 9 × 9 px square, while the integral is unity. The color map is shown for the normalized array. The minimum and maximum values in the real array are, respectively, 0.980 and 1.021. The image shows the statistical noise of the beam, which is doubled as a result of the division, whereas the ratio itself is close to unity.

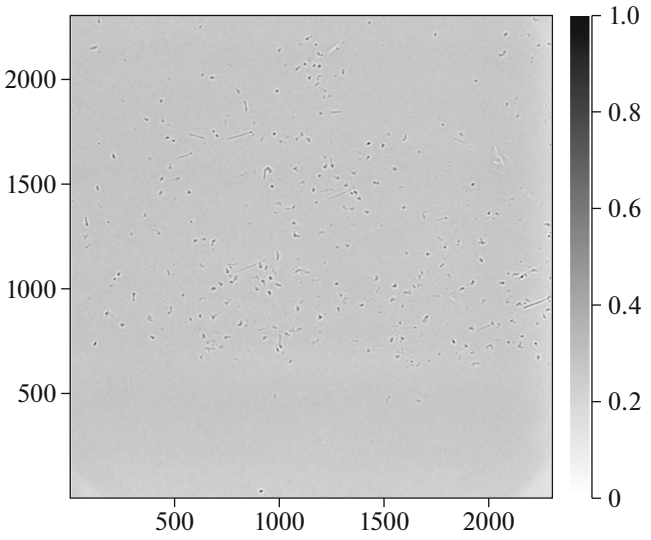

Fig. 4. Image of defects in a 1-mm-thick diamond crystal. The ratio of detector readings for the crystal studied and for the beam with approximately the same exposure in the absence of crystal, after averaging the matrix by calculating the convolution with the matrix whose values differ from zero and equal to each other in a 9 × 9 px square and the integral is unity, is presented. The color map is shown for the normalized array. The minimum and maximum values in the real array are, respectively, 0.811 and 1.399.

features of the dark detector disappear as a result of the division, but this occurs only when the SR beam intensity is fairly high. In this case, the maximum was at a level of 50000.

The diamond crystal, shaped as a plate, was 9 × 8 mm^2 in size and thus could not be exposed entirely to the SR beam. For this reason, 132 images of different crystal regions were obtained, which showed most various details, the analysis of which are beyond the scope of this study. Figure 4 presents only one region, containing many relatively small images, representing a dark spot, surrounded by a bright shell. There are almost round images with a diameter of ~30 px. Obviously, this is the result of SR beam minifocusing by a void with a round cross section ~10 μm in size. This image is shown after dividing the crystal matrix by the matrix of the empty beam with approximately the same exposure and after averaging over 9 px, as in Fig. 2. With allowance for the degree of beam coherence, this averaging barely deteriorates the object image sizes but suppresses essentially the statistical noise.

The total matrix contrast (0.266) significantly exceeds the empty beam contrast. For this reason the result is reliable; the empty beam contrast is also present here, but it is smaller by a factor of 10. The origin of the aforementioned defects is not yet known. They may be located both in the crystal bulk and on the surface. The latter situation is more likely; however, the crystal should be additionally investigated to answer this question. Our purpose was only to demonstrate the potential of phase-contrast microscopy for studying crystals.

CONCLUSIONS

An experiment on studying the defects in an artificial diamond crystal, obtained by chemical vapour deposition (CVD), was carried out. The study was performed by phase-contrast microscopy on the Pohang Light Source (Pohang, Republic of Korea). The specific features and problems of these measurements are discussed, in particular, dark detector readings (i.e., without illumination by the SR beam), analysis of the contrast related to the statistical noise in the SR beam, and elimination of the nonuniform intensity distribution in the incident beam. The measurements showed that the crystal has most various defects, including local defects ~10 μm in size. The data obtained suggest that it is expedient to use phase-contrast microscopy for crystal diagnostics.

FUNDING

This work was performed within the State assignment for the National Research Centre "Kurchatov Institute" and the State assignment for the Ioffe Institute of the Russian Academy of Sciences.

CONFLICT OF INTEREST

The authors of this work declare that they have no conflicts of interest.

REFERENCES

1. A. Snigirev, I. Snigireva, V. Kohn, et al., Rev. Sci. Instrum. **6** (12), 5486 (1995). https://doi.org/10.1063/1.1146073
2. P. Cloetens, R. Barrett, J. Baruchel, et al., J. Phys. D: Appl. Phys. **29** (1), 133 (1996). https://doi.org/10.1088/0022-3727/29/1/023
3. V. V. Lider and M. V. Koval'chuk, Crystallogr. Rep. **58**, 769 (2013). https://doi.org/10.1134/S1063774513050064
4. Y. Hwu, W. L. Tsai, A. Groso, et al., J. Phys. D: Appl. Phys. **35** (13), R105 (2002). https://doi.org/10.1088/0022-3727/35/13/201
5. R. Meuli, Y. Hwu, J. Je, et al., Eur. Radiol. **14** (9), 1550 (2004). https://doi.org/10.1007/s00330-004-2361-x
6. J. S. Lee, B. M. Weon, S. J. Park, et al., Sci. Rep. **14** (9), 1550 (2004). https://doi.org/10.1007/s00330-004-2361-x
7. G. Margaritondo and Y. Hwu, J. Imaging **7** (8), 132 (2021). https://doi.org/10.3390/jimaging7080132
8. J. Gastaldi, L. Mancini, E. Reinier, et al., J. Phys. D: Appl. Phys. **32** (10A), A152 (1999). https://doi.org/10.1088/0022-3727/32/10A/331
9. S. Agliozzo and P. Cloetens, J. Microsc. **216** (1), 62 (2004). https://doi.org/10.1111/j.0022-2720.2004.01385.x
10. V. G. Kohn, T. S. Argunova, and J. H. Je, Appl. Phys. Lett. **91**, 171901 (2007). https://doi.org/10.1063/1.2801355
11. V. G. Kohn, T. S. Argunova, and J. H. Je, J. Phys. D: Appl. Phys. **43**, 442002 (2010). https://doi.org/10.1088/0022-3727/43/44/442002
12. V. G. Kohn, T. S. Argunova, and J. H. Je, AIP Adv. **4**, 097134 (2014). https://doi.org/10.1063/1.4896512
13. V. G. Kohn, T. S. Argunova, and J. H. Je, Phys. Status Solidi B **255**, 1800209 (2018). https://doi.org/10.1002/pssb.201800209
14. T. S. Argunova and V. G. Kohn, Phys.-Uspekhi **62**, 602 (2019). https://doi.org/10.3367/UFNe.2018.06.038371
15. S. Zabler, H. Riesemeier, P. Fratzl, et al., Opt. Express **14** (19), 8584 (2006). https://doi.org/10.1364/OE.14.008584
16. P. Zaslansky, S. Zabler, and P. Fratzl, Dental Mater. **26** (1), e1 (2010). https://doi.org/10.1016/j.dental.2009.09.007
17. T. S. Argunova, V. G. Kohn, J.-H. Lim, et al., Phys. Lett. A **525**, 129901 (2024). https://doi.org/10.1016/j.physleta.2024.129901
18. T. S. Argunova, V. G. Kohn, J.-H. Lim, et al., Phys. Solid State **66**, 2108 (2024). https://doi.org/0.61011/PSS.2024.12.60201.6479PA
19. T. S. Argunova, V. G. Kohn, B. S. Roshchin, et al., Mater. Phys. Mech. **52** (5), 64 (2024). https://doi.org/10.18149/MPM.5252024_7
20. T. S. Argunova, V. G. Kohn, J. H. Lim, et al., J. Surf. Invest.: X-ray, Synchrotron Neutron Tech. **18 (**Suppl. 1), S16 (2024). https://doi.org/10.1134/S1027451024701817
21. C. Yu. Martyushov, I. L. Shul'pina, A. A. Lomov, et al., Phys. Solid State **65** (11), 1793 (2023). https://doi.org/10.61011/FTT.2023.11.56540.154
22. V. G. Kohn (2025). https://kohnvict.ucoz.ru/vkacl/ACLnews.htm

Translated by Yu. Sin'kov